SEPARATIONS

Nonequilibrium Cell Model for Packed Distillation Columns—The Influence of Maldistribution

Arnoud Higler,[†] R. Krishna,[‡] and Ross Taylor*[,†,§]

Department of Chemical Engineering, Clarkson University, Potsdam, New York 13699-5705; Department of Chemical Engineering, University of Amsterdam, Nieuwe Achtergracht 166, 1018 WV, Amsterdam, The Netherlands; Department of Chemical Engineering, University of Twente, Postbus 217, 7500 AE, Enschede, The Netherlands

In this paper we present a nonequilibrium model for studying the effects of flow maldistribution in packed columns. The model consists of a set of mass and energy balances along with a set of mass- and energy-transfer correlations. Maldistribution is treated by means of the zone/stage approach, as developed by Zuiderweg et al.[1] Simulations show that, for binary mixtures, packing HETPs are a function of the height of the packing. It should be noted that in some cases the behavior of HETPs is not intuitive, even for binary mixtures. For ternary mixtures, cases were found in which differences in maldistribution patterns can result in substantial differences in column behavior; in some cases completely different column products can be obtained.

1. Introduction

One of the main reasons for inadequate performance of packed columns is maldistribution of the internal vapor and liquid flows over the cross-sectional area of a column. Vapor and liquid channeling result in a loss of interfacial area and thereby considerably reduce the efficiency of the packing. Often these effects cannot be avoided, since the packing itself usually is one of the main causes for maldistribution. Liquid rivulets will form in any commercial packing, following specific paths. These rivulets will mix with other streams and split up again, thereby introducing small scale irregularities. The formation of rivulets, which mix and later split and mix again, is really the ideal way in which the liquid should flow down a (random) packed structure. The mechanism of frequent mixing and splitting leads to improvement in mass transfer; this is based on the rivulet model for mass transfer developed by Porter[2] in the 60s. According to Hoek et al.[3] the detrimental effects of this type of maldistribution largely are compensated by radial mixing. More detrimental is the so-called large scale maldistribution that may be caused by, among other things, changes in packing isotropy, most notably at the column wall, and a bad initial distribution of either phase. Stoter[4] presented substantial experimental evidence indicating a strong dependence of the packing HETP on maldistribution. Extensive discussions on the nature of these large scale maldistributions are given by Hoek et al.,[3] Stikkelman,[5] Stoter et al.,[6] and Stoter.[4]

1.1. Characterization.

One of the parameters most commonly used for quantifying the maldistribution is the coefficient of variation for the velocity profile C_v.[7]

$$C_v = \sqrt{\frac{1}{A_t}\int\left(\frac{u-\bar{u}}{\bar{u}}\right)^2 \mathrm{d}A} \tag{1}$$

where A_t is the total cross-sectional area of the column and the mean velocity $\bar{u}$ is calculated by

$$\bar{u} = \frac{1}{A_t}\int u \,\mathrm{d}A \tag{2}$$

Perry et al.[8] state that a C_v of less than 0.1 for distributors is adequate, provided that the deviations are randomly dispersed. Furthermore, it is assumed that the detrimental effects of small scale maldistributions are compensated for by radial mixing. Therefore, there is no need to take these into account in the evaluation of C_v.

In the most common approach for calculation of C_v, the cross-sectional area of a column is split up into a number of cells. The cell size is then chosen in such a way that variations in the velocity profiles within the cell are compensated for by radial mixing. The value of C_v may then be determined by

$$C_v = \sqrt{\frac{1}{A_t}\sum_{i=1}^{N} A_i\left(\frac{u_i-\bar{u}}{\bar{u}}\right)^2} \tag{3}$$

where N is the total number of cells and $\bar{u}$ is the average velocity over the entire cross-sectional area, which may be determined by

* To whom all correspondence should be addressed. Telephone: 315-268-6652. Fax 315-268-6654. E-mail: taylor@clarkson.edu.
[†] Clarkson University.
[‡] University of Amsterdam.
[§] University of Twente.

10.1021/ie990261l CCC: $18.00
Published on Web 08/28/1999

$$\bar{u} = \frac{1}{A_t}\sum_{i=1}^{N} A_i \cdot u_i \tag{4}$$

This coefficient of maldistribution does not, however, take into account possible clustering of large scale maldistributions. An alternative "coefficient of maldistribution" was devised by Billingham et al.[7] This new coefficient C_m is evaluated in very much the same way as C_v except that the local mean velocity, rather than the overall mean velocity, is used. The coefficient of variation for a cell configuration is given by

$$C_m = \sqrt{\frac{1}{A_t}\sum_{i=1}^{N} A_i \left(\frac{u_i - \bar{u}_i}{\bar{u}_i}\right)^2} \tag{5}$$

Here $\bar{u}$ is the local mean velocity, which is calculated from

$$\bar{u}_i = \frac{\sum \delta_{ij}(A_i u_i + A_j u_j)}{\sum \delta_{ij}(A_i + A_j)} \tag{6}$$

where $\delta_{ij} = 1$ if i and j are neighbors, and $\delta_{ij} = 0$ if i and j are not located next to each other. One should note here that when flow variations are about uniformly distributed over the cross-sectional area, the values of C_v and C_m do not differ very much. However, if the maldistributions are clustered, the value of C_m will be much lower than the value of C_v. For simplification of the interpretation, a Maldistribution Index MI is introduced[7] and defined by

$$MI = \frac{C_v}{C_m} \tag{7}$$

This maldistribution index is a measure of the clustering of maldistributions. If MI is close to unity, maldistributions will be distributed evenly over the cross-sectional area. A larger value of MI indicates clustering of the large scale maldistributions.

The above methods help to characterize the initial flow maldistributions, but they do not provide much insight into the depth to which the maldistribution persists. This was pointed out by Edwards et al.,[9] who developed a method for the prediction of the maldistribution depth of penetration l_m. This is defined as the depth into the packing over which the coefficient of variation exceeds a design limit. The method is based on solving a simplified flow model and is strongly correlated to the maldistribution index of Billingham et al.[7] These indices do give some indication on the degree of maldistribution of the phases in a packed column. However, they do not say anything about the effect of these maldistributions on the packing efficiency and, hence, on the distillation process.

1.2. Maldistribution and Packing Efficiency. Partly on the basis of on the results of the work by Hoek et al.,[3] Stikkelman,[5] and Stoter,[4] Zuiderweg et al.[1] developed a "zone/stage" model for estimation of the overall efficiency of a packed column, given a specific initial maldistribution of the liquid phase. The model has two independent calculation steps. The first step calculates the liquid maldistribution on the basis of on a natural flow model as outlined by Stikkelman.[5] In the second step, the influence of this maldistribution on the HETP (height equivalent of a theoretical plate), and thereby on the packing efficiency, is determined.

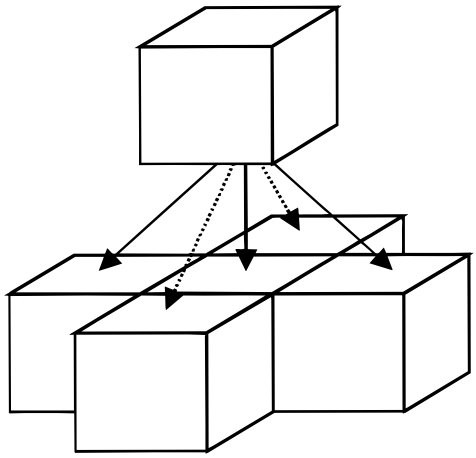

Figure 1. Flow splitting pattern in zone/stage model.

The effect of the maldistribution on the flow pattern is determined by means of a cell model, whereby it is assumed that a fraction K^L of the liquid leaving the cell will flow down to the cell below. The remaining fraction of liquid $(1 - K^L)$ will flow to the adjacent cells below, whereby the flows are split up according to the ratio of the cell surface areas between the cells. The resulting flow pattern is shown in Figure 1. This is referred to as the natural flow model. The underlying idea of the natural flow model is that a liquid flowing down a section of packing will spread according to a diffusional type equation:

$$\frac{\partial u}{\partial z} = D_r\left(\frac{1}{r}\frac{\partial u}{\partial r} + \frac{\partial^2 u}{\partial r^2}\right) \tag{8}$$

where D_r is a liquid spreading coefficient. Bemer and Zuiderweg[10] show that

$$r^2 = -4D_r z \ln(1 - x) \tag{9}$$

in which r represents the radius of a circle at a distance z below a liquid point source, through which a fraction x of the injected liquid flows. Hoek et al.[3] measured the spreading coefficient for various types of packing and found that the spreading coefficient is strongly dependent on the type of packing and the packing size. Billingham et al.[7] suggest values for the radial spreading coefficients for various types of packing:

1st generation random packings	$D_r = 0.12 d_p$
2nd generation random packings	$D_r = 0.06 d_p$
structured packing	$D_r = 0.0035$

where d_p is the packing size in meters.

Stikkelman[5] carried out point source calculations for the outlined flow pattern using a random walk model. His calculations suggest the following relationship for the splitting factor K^L and the liquid spreading coefficient D_r:

$$(1 - K^L) = 4 \cdot \frac{D_r \cdot z_l}{r_l^2} \tag{10}$$

Here r_l is the spreading distance, which corresponds to the cell width, and z_l is the layer height. According to Zuiderweg et al.,[1] the zone stage model is compatible with the diffusion flow model only if $K^{L} = {}^{2}/_{3}$. Furthermore, eq 10 is only valid for cell layout patterns as presented in Figure 1. Zuiderweg et al.[1] present a cell model consisting of annular concentric cells. For this model

$$(1 - K^{L}) = 2 \cdot \frac{D_r \cdot z_l}{r_l^2} \tag{11}$$

Once we have specified a packing type and height, and a number of stages, the number of zones required for a correct description of the zone stage model follows, when using square cells, from eq 10. For a radial model, the cell width follows from eq 11. Zuiderweg et al.[1] go on to show that, for a given packing type and size, number of cells, and column width, there is a single value for the layer height satisfying the diffusion equation. From that height he then derives his "adjusted HETP" by means of equilibrium calculations.

With respect to the cell sizes and splittting factors, we have to keep in mind that in practice they will be different for columns of different aspect ratios. For small diameter columns, the development of maldistributions along the height of the packing will be different than that for columns with a larger diameter. In addition, for small diameter columns, the influence of the wall is much more important than that for large diameter columns.

Nawrocki et al.[11] present a model for determining the influence of maldistribution in structured packings. Their approach uses empirical correlations for the interfacial area and mass-transfer coefficients modified by taking into account flow mixing and splitting on the crossover length scale. As Zuiderweg et al.[1] point out, such models can lead to very tedious calculations for commercial size columns, as there are thousands of crossovers in a column cross section. On this scale radial mixing compensates largely for maldistribution and this eliminates the need for modeling on the crossover scale.

From all of the above papers we can conclude that there is an understanding of flow maldistribution in packing and that there are models that appear adequate for describing the development of these large scale maldistributions. In addition, there is general agreement, and sufficient evidence, to support the statement that maldistribution has a detrimental effect on column performance. However, there is no direct method available for determining the influence of these maldistributions, particularly for multicomponent systems. The method of Zuiderweg et al.[1] requires two calculation steps and has a number of drawbacks. First, it does not take into account the effect of local flow on the interfacial area. This is, however, one of the main reasons for bad behavior. Second, it does not take into account the differences in residence times for various maldistribution flows along the column. Furthermore, the method requires one to use the HETP concept, which in itself can be very confusing when used in multicomponent systems.[12]

In this paper we present a more direct approach for evaluating the influence of flow maldistribution on the distillation process. Here, we use the zone stage flow model, as presented by Zuiderweg et al.[1] However, instead of just using it to determine the flow patterns, we will assume each cell to be a nonequilibrium vapor/liquid contacting cell. Flow maldistributions are evaluated by means of the linking pattern, and the effects of this maldistribution on mass transfer are directly evaluated inside the nonequilibrium cells. This way, one can directly calculate the influence of large scale flow maldistributions on the distillation process, without having to revert to HETPs.

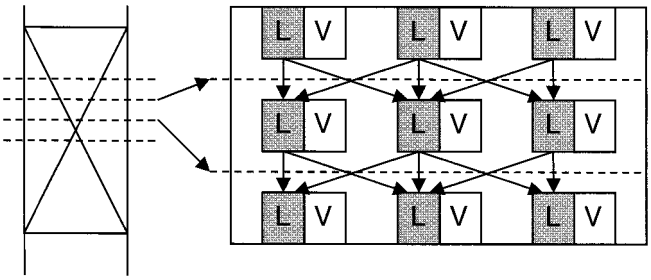

Figure 2. Schematic representation of nonequilibrium cell model for packed columns.

2. Nonequilibrium Zone Stage Model

For the nonequilibrium zone stage model we assume that a section of packing may be "sliced" into a number of stages. This is common practice for any nonequilibrium model for packed columns. We now divide each slice into a number of cells or zones. This is illustrated in Figure 2.

Here, only the flow paths for the liquid are given. Similar patterns can be drawn for the vapor streams. In addition, there will be cells in front of and behind the given cells, resulting in a three-dimensional flow model rather than the two-dimensional representation that is shown in the illustration.

2.1. Stage Equations. For each "slice" or "stage" we can write a set of mass and energy conservation equations that organizes the calculation of the interstage flows. For each stage we have

$$(1 + r_j^{L}) \cdot L_j^{S} - \sum_{k=1}^{n^z} L_k^{C} = 0 \tag{12}$$

in which L_j^{S} represents the stage liquid flow leaving stage j and L_k^{C} represents the liquid flows coming from the cells on stage j. n^{Z} is the number of cells on a stage, and r_j^{L} is the ratio of the liquid side stream flow rate to the stage liquid flow rate. r_j^{L} is not zero only if stage j has a liquid side drawoff. Similarly, we have an expression for the stage vapor flow.

$$(1 + r_j^{V}) \cdot V_j^{S} - \sum_{k=1}^{n^z} V_k^{C} = 0 \tag{13}$$

Here, V_j^{S} is the stage vapor flow leaving stage j and V_k^{C} is the vapor flow coming from cell k on stage j. In addition we have the stage component balance equations for the liquid and vapor phases, respectively. r_j^{V} is the vapor side drawoff ratio, which is nonzero if stage j has a vapor side drawoff.

$$(1 + r_j^{L}) \cdot x_{i,j}^{S} \cdot L_j^{S} - \sum_{k=1}^{n^z} x_{i,k}^{C} \cdot L_k^{C} = 0 \tag{14}$$

$$(1 + r_j^{\mathrm{V}})\cdot y_{i,j}^{\mathrm{S}}\cdot V_j^{\mathrm{S}} - \sum_{k=1}^{n^z} y_{i,k}^{\mathrm{C}}\cdot V_k^{\mathrm{C}} = 0 \qquad (15)$$

In the above equations, $x_{i,j}^{\mathrm{S}}$ and $y_{i,j}^{\mathrm{S}}$ are the liquid and vapor mole fractions of component i leaving stage j. $x_{i,k}^{\mathrm{C}}$ and $y_{i,k}^{\mathrm{C}}$ are the liquid and vapor phase mole fractions of component i leaving cell k. In addition we have the enthalpy balance equations for each phase.

$$(1 + r_j^{\mathrm{L}})\cdot H_j^{\mathrm{SL}}\cdot L_j^{\mathrm{S}} - \sum_{k=1}^{n^z} H_k^{\mathrm{CL}}\cdot L_k^{\mathrm{C}} = 0 \qquad (16)$$

$$(1 + r_j^{\mathrm{V}})\cdot H_j^{\mathrm{SV}}\cdot V_j^{\mathrm{S}} - \sum_{k=1}^{n^z} H_k^{\mathrm{CV}}\cdot V_k^{\mathrm{C}} = 0 \qquad (17)$$

H_j^{SL} and H_j^{SV} are the liquid and vapor enthalpies of the streams leaving the stage. H_k^{CL} and H_k^{CV} are the enthalpies of the streams leaving cell k on the stage. To complete the stage equations, we have the stage hydraulic equation.

$$p_j - p_{j-1} - (\Delta p_{j-1}) = 0 \qquad (18)$$

where p_j and p_{j-1} are the stage pressures on stages j and $j - 1$, respectively. Δp_{j-1} is the pressure drop per slice from stage $j - 1$ to stage j. The pressure drop over the stage is considered to be a function of the stage flows, the fluid physical properties (such as densities and surface tension), and the packing type. This completes the definition of the equations required for the stage flows, compositions, temperatures, and pressures.

2.2. Cell Equations. A schematic representation of a contacting cell is given in Figure 3. For each contacting cell we have the following equations: total mole (mass) balances for the liquid phase and the vapor phase.

$$L_{j,k}^{\mathrm{C}} - K^{\mathrm{L}}\cdot L_{j-1,k}^{\mathrm{C}} - \sum_l (1 - K^{\mathrm{L}})\cdot r_{\mathrm{a}}^{\mathrm{L}}\cdot L_{j-1,l}^{\mathrm{C}} - r_{\mathrm{f}}^{\mathrm{L}}\cdot F_j^{\mathrm{SL}} - N_{\mathrm{t},k}^{\mathrm{L}} = 0 \qquad (19)$$

$$V_{j,k}^{\mathrm{C}} - K^{\mathrm{V}}\cdot V_{j+1,k}^{\mathrm{C}} - \sum_l (1 - K^{\mathrm{V}})\cdot r_{\mathrm{a}}^{\mathrm{V}}\cdot V_{j+1,l}^{\mathrm{C}} - r_{\mathrm{f}}^{\mathrm{V}}\cdot F_j^{\mathrm{SV}} + N_{\mathrm{t},k}^{\mathrm{V}} = 0 \qquad (20)$$

Here K^{L} is the liquid splitting factor, which represents the fraction of liquid from a cell that goes to the cell directly below. K^{V} is the fraction of vapor that goes to the cell directly above. The summation terms indicate the incoming terms from all the adjacent cells, whereby the factors $r_{\mathrm{a}}^{\mathrm{L}}$ and $r_{\mathrm{a}}^{\mathrm{V}}$ determine how much of the mixing flows that leave the adjacent cells enter the cell under consideration. This will be discussed in more detail in a subsequent section. F_j^{SL} and F_j^{SV} represent feed streams to the stage under consideration. The factors $r_{\mathrm{f}}^{\mathrm{L}}$ and $r_{\mathrm{f}}^{\mathrm{V}}$ determine the fraction of the feed that enters the cell under consideration. This will also be discussed in more detail in a following section. $N_{\mathrm{t},k}^{\mathrm{L}}$ and $N_{\mathrm{t},k}^{\mathrm{V}}$ are the total mass-transfer rates in the vapor and liquid phases. The total mass-transfer rates are obtained by summing up over the individual component mass-transfer rates.

Along with the overall mass balance we have the component mass balances. For each component we can write for the vapor and liquid phases

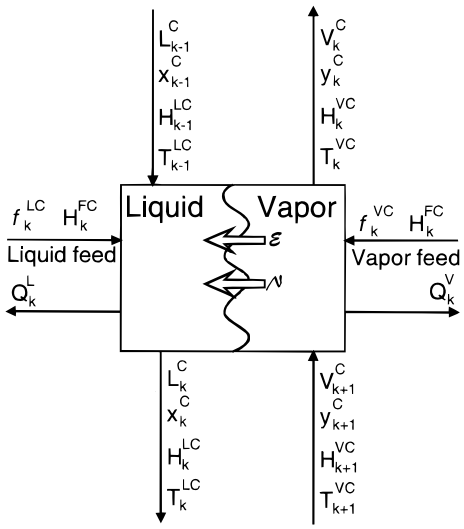

Figure 3. Schematic representation of a nonequilibrium cell.

$$x_{i,j,k}^{\mathrm{C}}\cdot L_{j,k}^{\mathrm{C}} - K^{\mathrm{L}}\cdot x_{i,j-1,k}^{\mathrm{C}}\cdot L_{j-1,k}^{\mathrm{C}} - \sum_l (1 - K^{\mathrm{L}})\cdot r_{\mathrm{a}}^{\mathrm{L}}\cdot x_{i,j-1,l}^{\mathrm{C}}\cdot L_{j-1,l}^{\mathrm{C}} - r_{\mathrm{f}}^{\mathrm{L}}\cdot f_{i,j}^{\mathrm{SL}} - N_{i,k}^{\mathrm{L}} = 0 \qquad (21)$$

$$y_{i,j,k}^{\mathrm{C}}\cdot V_{j,k}^{\mathrm{C}} - K^{\mathrm{V}}\cdot y_{i,j+1,k}^{\mathrm{C}}\cdot V_{j+1,k}^{\mathrm{C}} - \sum_l (1 - K^{\mathrm{V}})\cdot r_{\mathrm{a}}^{\mathrm{V}}\cdot y_{i,j+1,l}^{\mathrm{C}}\cdot V_{j+1,l}^{\mathrm{C}} - r_{\mathrm{f}}^{\mathrm{V}}\cdot f_i^{\mathrm{SV}} + N_{i,k}^{\mathrm{V}} = 0 \qquad (22)$$

In the above equations, $x_{i,j,k}^{\mathrm{C}}$ represents the liquid mole fraction of component i in cell k on stage j, $y_{i,j,k}^{\mathrm{C}}$ is the vapor mole fraction of component i on stage j in cell k. $f_{i,j}^{\mathrm{L}}$ is the total liquid feed of component i on stage j, and $f_{i,j}^{\mathrm{V}}$ is the total vapor feed of component i on stage j. The individual component mass-transfer rates are related to chemical potential gradients by the generalized Maxwell−Stefan equations.[13,14]

$$\frac{x_{i,k}}{RT_k}\frac{\partial \mu_{i,k}^{\mathrm{L}}}{\partial \eta} = \sum_{l=1}^{c}\frac{x_{i,k}N_{l,k}^{\mathrm{L}} - x_{l,k}N_{i,k}^{\mathrm{L}}}{c_{\mathrm{t},k}^{\mathrm{L}}(\kappa_{i,l}^{\mathrm{L}}a)_k} \qquad (23)$$

$$\frac{y_{i,k}}{RT_k}\frac{\partial \mu_{i,k}^{\mathrm{V}}}{\partial \eta} = \sum_{l=1}^{c}\frac{y_{i,k}N_{l,k}^{\mathrm{V}} - y_{l,k}N_{i,k}^{\mathrm{V}}}{c_{\mathrm{t},k}^{\mathrm{V}}(\kappa_{i,l}^{\mathrm{V}}a)_k} \qquad (24)$$

In these equations, R is the gas constant, μ_i is the chemical potential of species i, η is a dimensionless film coordinate, $c_{\mathrm{t},k}^{\mathrm{L}}$ is the total liquid-phase concentration, and $c_{\mathrm{t},k}^{\mathrm{V}}$ is the total vapor phase concentration. $\kappa_{i,l}^{\mathrm{L}}a$ and $\kappa_{i,l}^{\mathrm{V}}a$ are the liquid and vapor phase volumetric mass transfer coefficients, respectively. Only $c - 1$ of these equations are independent. The mole fraction of the c-th component is obtained from the mole fraction summation equation for the appropriate phase.

The enthalpy balance equations for both phases are

$$H_{,j,k}^{\mathrm{CL}}\cdot L_{j,k}^{\mathrm{C}} - K^{\mathrm{L}}\cdot H_{j-1,k}^{\mathrm{CL}}\cdot L_{j-1,k}^{\mathrm{C}} - \sum_l (1 - K^{\mathrm{L}})\cdot r_{\mathrm{a}}^{\mathrm{L}}\cdot H_{j-1,l}^{\mathrm{CL}}\cdot L_{j-1,l}^{\mathrm{C}} - r_{\mathrm{f}}^{\mathrm{L}}\cdot H_j^{\mathrm{FL}}\cdot F_j^{\mathrm{SL}} - \epsilon_k^{\mathrm{L}} + Q_K^{\mathrm{L}} = 0 \qquad (25)$$

$$H^{CV}_{j,k}\cdot V^{C}_{j,k} - K^{V}\cdot H^{CV}_{j+1,k}\cdot V^{C}_{j+1,k} - \sum_{l}(1 - K^{V})\cdot r^{V}_{a}\cdot H^{CV}_{j+1,l}\cdot V^{C}_{j+1,l} - r^{V}_{f}\cdot H^{FV}_{j}\cdot F^{SV}_{j} + \epsilon^{V}_{k} + Q^{V}_{K} = 0 \quad (26)$$

The energy-transfer rates consist of convective and conductive contributions. For the liquid and vapor phases we have

$$\epsilon^{L}_{k} = -h^{L}_{k}\cdot a\cdot\frac{\partial T^{L}}{\partial \eta} + \sum_{i=1}^{c} N^{L}_{i,k} H^{L}_{i,k} \quad (27)$$

$$\epsilon^{V}_{k} = -h^{V}_{k}\cdot a\cdot\frac{\partial T^{V}}{\partial \eta} + \sum_{i=1}^{c} N^{V}_{i,k} H^{V}_{i,k} \quad (28)$$

Here h^{L}_{k} and h^{V}_{k} are the volumetric heat-transfer coefficients for the liquid and vapor phases. For the energy-transfer rates we have

$$\epsilon^{L}_{i,k} = \epsilon^{V}_{i,k} \quad (29)$$

This equation plays a very important role in determining the mass-transfer rates. The Maxwell−Stefan equations by themselves are "floating equations". They relate the driving force for mass transfer of a component to the friction of the other species on that component. This is done in terms of relative component velocities and therefore we need one extra equation to "tie down" these relative velocities. That is done by eq 29. This equation is commonly referred to as the "bootstrap" equation.[13,14]

At the vapor/liquid interface we assume phase equilibrium. For each component we have

$$y^{I}_{i,k} - K_{i,k}x^{I}_{i,k} = 0 \quad (30)$$

Here $y^{I}_{i,k}$ is the vapor phase composition at the interface and $x^{I}_{i,k}$ is the liquid-phase composition at the interface. $K_{i,k}$ is the vapor−liquid equilibrium ratio for component i in cell k and is a function of interface temperatures and concentrations and stage pressure. In addition, it is necessary that all the interface mole fractions should sum up to one for both phases.

2.3. Solving the Model Equations. For solving the model equations, the derivatives in the mass- and heat-transfer equations (eqs 17, 23, 24, and 28) are replaced by finite difference approximations. For more details, see Higler et al.[15] The resulting set of algebraic equations is solved using Newton's method, as outlined by Taylor et al.[16]

2.4. Hydrodynamic Equations. The objective of a nonequilibrium model is to describe what happens in an actual piece of process equipment. Because various model parameters, such as the interfacial area, the mass-transfer coefficients, and the pressure drop depend on the internals used in the process equipment, seemingly, a nonequilibrium model cannot proceed without information about the actual design. This would greatly limit the applicability of a nonequilibrium model. Therefore we have equipped our nonequilibrium model with a "design mode", that evaluates a column design, on the basis of a specified internal type and the estimated model parameters and physical properties during the iterations. This design is used in calculation of the hydrodynamic and mass-transfer parameters in the next iteration. After each iteration, the design is checked, and updated if necessary. After convergence is achieved, we have a design that is consistent with the solution of the model. It should be emphasized that the design obtained this way is not optimized. However, it serves as a working solution and can be used as a starting point for further optimization. The design mode was used in our examples to generate a design for our column simulations.

When using a zone/stage description of a distillation column, one should keep in mind that local differences in concentrations and flow densities and so forth will lead to local differences in various hydrodynamic parameters as well: most notably the vapor/liquid interfacial areas and holdups, and to a lesser extent the mass-transfer coefficients. For calculation of the mass-transfer rates, local differences of the last two factors may safely be neglected. It has often been stated that the detrimental effect of maldistribution in packed columns is largely due to the loss of interfacial area due to liquid and vapor channeling. For correct prediction of column behavior it is, therefore, important to evaluate the vapor/liquid interfacial area for each cell individually. In the proposed model, the interfacial areas are evaluated for each cell using local cell flow rates and averaged physical properties.

The approach outlined above will allow us to model maldistribution only to a certain extent. The most common correlations for interfacial areas, holdups, and so forth were not derived and were not meant to be applied to the hydrodynamic conditions that will arise locally in cases of severe maldistribution. The model is, therefore, applicable only to cases of moderate maldistribution, in which we do not have complete flooding or drying of the packing.

In addition, the fact that flow profiles are generated on the basis of an imposed flow-splitting policy means that we cannot account for changes in vapor flow profiles due to maldistributed liquid flows and vice versa.

2.5. Specifications. The most likely sources for maldistribution of vapor and liquid are found at inlets: most notably the reflux inlet and, to a lesser extent, the liquid feed inlet. In the zone/stage model, as presented, we assume, in the ideal case, that reflux, reboil, and feed streams are distributed equally over the cross-sectional area of the packing. Maldistributions may now be introduced by redirecting the flow according to specified maldistribution patterns. This may be done by assigning weighing factors to the values of r^{L}_{f} and r^{V}_{f} in eqs 19−26. Classification of maldistribution is described above. We only need to make sure that the cell size in our zone/stage model is such that the resulting flow model is consistent with eq 8.

3. Cell Models

3.1. Radial Model. In the classical zone/stage model, as presented by Zuiderweg et al.,[1] it is assumed that a stage is split up in a number of annular zones. This is illustrated in Figure 4. A fraction K^{L} out of the liquid stream in every zone flows downward, while the remaining fraction flows sideways to the adjacent zones. The flow coming in from the adjacent cells has to be weighted by the ratio of the "inside" and "outside" interfacial areas of the cell. If the liquid comes from the "inner" annular space, we need to multiply the flow by the relative fraction of the "outside area" of the inner annular space. This is given by

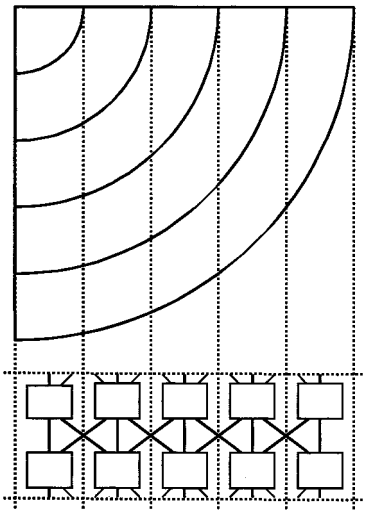

Figure 4. Radial mixing model for maldistribution.

$$r_k^{ao} = \frac{a_k}{a_k + a_{k-1}} = \frac{r_k}{r_k + r_{k-1}} = \frac{k}{2k-1} \qquad (31)$$

Similarly, if the liquid comes from the cell "outside" the cell under consideration, we have to multiply by the "inside area fraction" of the cell.

$$r_k^{ai} = \frac{a_{k-1}}{a_k + a_{k-1}} = \frac{r_{k-1}}{r_k + r_{k-1}} = \frac{k-1}{2k-1} \qquad (32)$$

Thus, the summation term in eq 19 becomes

$$\sum_l (1 - K^L)\cdot r_a^L \cdot L_{j-1,l}^C = (1 - K^L)\cdot(L_{k-1,j-1}\cdot r_{k-1}^{ao} + L_{k+1,j-1}\cdot r_{k+1}^{ai}) = 0 \qquad (33)$$

Furthermore, it is assumed, in the ideal case, that any liquid feed will be distributed equally over the cross-sectional area of the column. Therefore, only a fraction, r_f^L, which is the ratio of the cross-sectional annular area to the total column cross-sectional area, will be supplied to cell k on stage j. r_f^L is given by

$$r_f^L = \frac{\pi r_k^2 - \pi r_{k-1}^2}{\pi R^2} = \frac{k^2 - (k-1)^2}{(n^Z)^2} = \frac{2k-1}{(n^Z)^2} \qquad (34)$$

Similar considerations apply to the vapor phase.

3.2. Square Grid Model. It may be clear that the radial model as outlined above may be used only for studying maldistributions that by themselves are radial. For studying other maldistribution patterns, we will use a square grid, in which we will have a flow distribution as depicted in Figure 1. The liquid from each square cell flows to five different cells on the next layer. Once again, we assume that a fraction K^L flows straight down to the cell directly below and a fraction $1 - K^L$ is split up in four streams. Of this latter fraction another fraction, K_x^L, is distributed equally over the two cells "east" and "west" of the cell under consideration. The other fraction $K_y^L = 1 - K_x^L$ is distributed equally over the cells "north" and "south" of the cell under consideration. For random packings, K_x will be 0.5, resulting in equal quantities going to all cells. For structured packings, there will be a preferred flow direction in either the north−south or east−west direction, resulting in different values of K_x^L and K_y^L. In a normal column with structured packing, the preferred flow direction of the packing will switch every so often. This can be taken into account by switching the values of K_x^L and K_y^L on the appropriate stages.

3.3. Maldistribution Patterns. In the following examples we will use various maldistribution patterns for the reflux streams supplied to the packing. A graphical representation is given in Figure 5. We assume that the superficial velocity of vapor or liquid supplied to the gray zones is three times the superficial velocity supplied to the white zones. The maldistribution patterns may be imposed on either the reboiled vapor stream or the liquid reflux stream to the column. In the following examples we will only consider maldistribution in the liquid stream.

The values of C_v and MI are given in Figure 5 as well. Models Radial-0 and Square-0 are our base cases, assuming no maldistribution. It should be noted that all of the square grid cases are axisymmetric and will be modeled by using just part of the column. However, it is quite simple to tackle nonaxisymmetric initial distributions with the model as described.

3.4. Redistribution. In practice, liquid will be redistributed over the cross-sectional area of the column every 2−4 m of packing, depending on packing type, flow conditions, and so forth. This is to ensure that possible maldistributions arising due to a bad initial distribution of the reflux or to packing anisotropy cannot propagate through the entire column. In our model we may redistribute the liquid at specified stages. Redistribution itself can also be a source of maldistribution, which may be modeled by specifying a maldistribution pattern for the redistributor.

4. Model Application

In this section we will illustrate the use of the nonequilibrium zone/stage model. We will study the influence of maldistribution on the packing efficiency for a random packing and for structured packing using a binary system. In addition we will study the influence of maldistribution on two ternary systems.

4.1. Random Packing. In this section we will focus on the effect on maldistribution on random packing. For simplicity we will use a binary system. This is because the HETP concept really only has a physical meaning for binary systems, and the component HETPs are, by definition, equal. For more than two components, the individual component HETPs usually are not equal and can behave oddly.[12]

Our case study is based on a column with a packed height of 6 m, which is split up into 60 slices, each of 0.1 m. The column has a total condenser and a partial reboiler. We assume that the column is packed with 2 in. Raschig rings. A liquid feed is supplied between stages 31 and 32 at a pressure of 506.6 kPa and a flow rate of 100 mol·s^{-1}. The feed is a 50/50 mixture of propane and *n*-butane. The Peng−Robinson equation of state is used for calculation of the thermodynamic properties. The mass-transfer coefficients and the interfacial area are calculated with the method of Onda et al.[17]

The column is operated at a reflux ratio of 2.5 and a bottom product flow rate of 50 mol·s^{-1}. From initial calculations in the design mode, using just a single zone per stage, we find that the column diameter is about

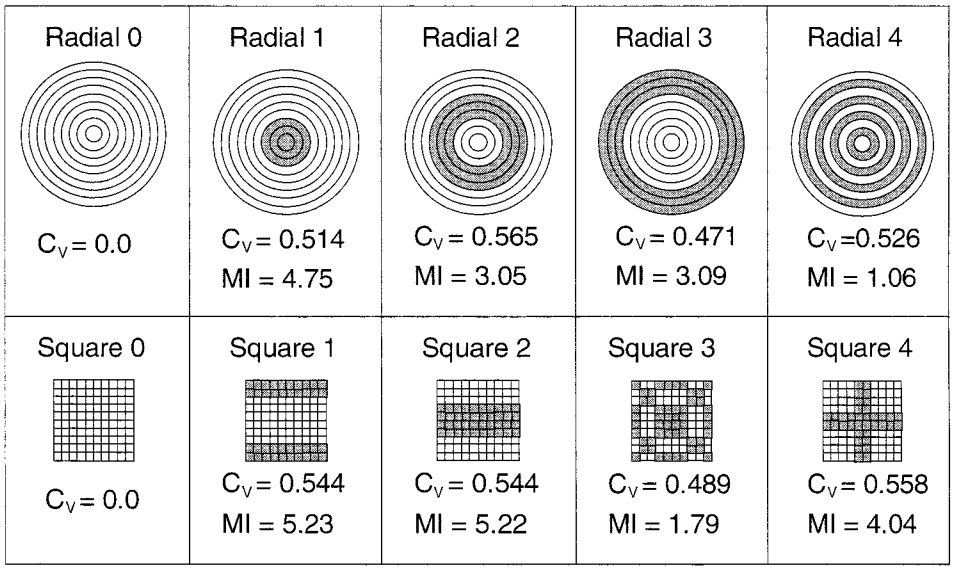

Figure 5. Maldistribution patterns.

1.1 m. In the remainder of the calculations, the column diameter was fixed at 1.1 m. From eq 10 we find that a cell width of about 0.085 m is required for a square grid problem. Assuming the cross-sectional area of the round column is equal to the cross-sectional area of the now square column, we need a 10 × 10 cell configuration. Since we consider our maldistribution patterns to be axisymmetric, a 5 × 5 configuration, with appropriate boundary conditions will suffice. For a radial model, eq 11 suggests that the required cell width is about 0.06 m and that we have to use nine annular zones for a correct description of maldistribution. In addition we will assume that the column internal flows will be perfectly redistributed every 2 m of packing. This corresponds to stages 20 and 40. In what follows we will focus our attention on the influence of maldistribution of the reflux on column behavior.

4.1.1. Results. For interpretation of the effect of the packing, we will have a look at the differential packing HETP, defined by

$$\mathrm{HETP}_i = H / E_i^{\mathrm{MV}} \tag{35}$$

where H is the height of the slice of packing under consideration (in this example $H = 0.1$ m), and E_i^{MV} is the Murphree vapor-phase efficiency of component i, calculated from the results of a nonequilibrium simulation by

$$E_i^{\mathrm{MV}} = \frac{\bar{y}_{i,j} - \bar{y}_{i,j+1}}{\bar{y}^*_{i,j} - \bar{y}_{i,j+1}} \tag{36}$$

Here $\bar{y}_{i,j}$ is the average composition of the vapor leaving the slice of packing under consideration, $\bar{y}^*_{i,j}$ is the average concentration of vapor that would be in equilibrium with the liquid phase on the stage under consideration and is obtained from a bubble point calculation of the liquid phase, and $\bar{y}_{i,j+1}$ is the average composition of the vapor exiting from the slice below. If the individual component efficiency equals 1, then the stage can be considered an equilibrium stage and the H corresponds to the HETP. The HETPs for the radial and axisymmetric cases are shown in Figures 6 and 7 for the 30 stages above the feed.

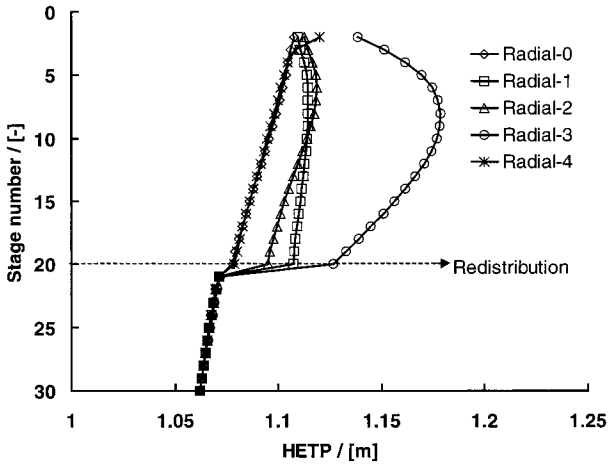

Figure 6. Differential HETPs for radial maldistribution cases.

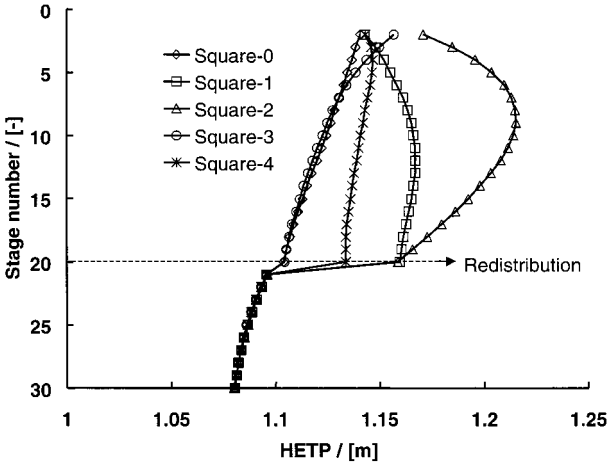

Figure 7. Differential HETPs for square grid maldistribution cases.

We can make a number of observations here. We see that the cases without maldistribution (Radial-0 and Square-0) are reasonably well behaved. The differences between the Square-0 and Radial-0 models are due to the differences in the column flow profiles, that arise in the natural flow model. The natural flow model does not predict a flat velocity profile over the cross section of the column. In the radial model, it is true that for

the inner cells we find a flat velocity profile; however, the velocity in the outer ring is lower. Similarly, in the square grid model, the velocities in the corner cells will be different from the velocities in the cells adjacent to the column wall, which in turn will have velocities different from those for cells that are fully surrounded by other cells. These "naturally" occurring different flow profiles give rise to the differences observed between the nonmal distributed cases Radial-0 and Square-0. It should be noted that normally one would expect higher velocities along the wall and lower velocities closer to the center of the column. This may easily be modeled by adopting different flow splitting factors. The same holds for wall effects in small diameter columns. By adjusting the cell sizes and splitting factors in an appropriate way, it is possible to impose any kind of flow profile to closely approximate what would be encountered in a real column.

In addition, we can see that there is some kind of correlation between the deviation of the HETP from the ideal case and the value of the maldistribution index *MI*. For a low value of *MI*, cases Radial-4 and Square-3, we find behavior that is very close to those for cases Radial-0 and Square-0. For the higher values, the deviations are larger. However, it is also clear that the predictive value of C_v and *MI* is suspect. This is illustrated by cases Square-1 and Square-2. Although these cases have almost the same values for C_v and *MI*, the HETP patterns are very different. This is probably due to wall effects that play a much more important role in case Square-1.

The effect of ideally redistributing the flow on stage 20 is clearly visible for both the square grid and the radial cases. As a result of the redistribution, the flow profiles on the stages below stage 20 will be the same for all cases and so will the mass-transfer characteristics (HETPs). Above the redistribution the average HETPs are, clearly, height dependent.

The overall effect of maldistribution is more complicated than can be summarized by a C_v and an *MI*. These parameters do give adequate information about the degree of maldistribution of the flow; however, they do not indicate how the maldistribution influences the column efficiency. It is usually true that maldistribution leads to reduced column efficiency. However, poorer maldistribution characteristics do not necessarily lead to degraded column performance.

4.2. Structured Packing. The development of maldistribution in sheet type structured packing requires some more attention. In sheet type packings, the direction of the channels formed by the sheets dictates a specific spreading direction. Sheets are packed together in a packing element, and a stack of these elements forms the column packing. The elements are placed such that the orientation of the flow direction in the adjacent elements changes by 90°. This means that after several layers of packing a good redistribution of both phases in all directions should occur.

In modeling the effect of maldistributions on the performance of structured packings, we need to take into account this change in orientation. This is particularly interesting for maldistribution cases whereby the initial maldistribution has the same orientation as the first layer of packing. This can be illustrated by looking at cases Square-1 and Square-2 in Figure 5. We assume that the first packing element has its sheets oriented along the maldistribution. In this case there will be hardly any exchange between the highly irrigated zone and the lower irrigated zones in the first packing element. This also means that, due to the higher loading, the interfacial area will be lower in the highly irrigated section, reducing the mass-transfer efficiency of this section.

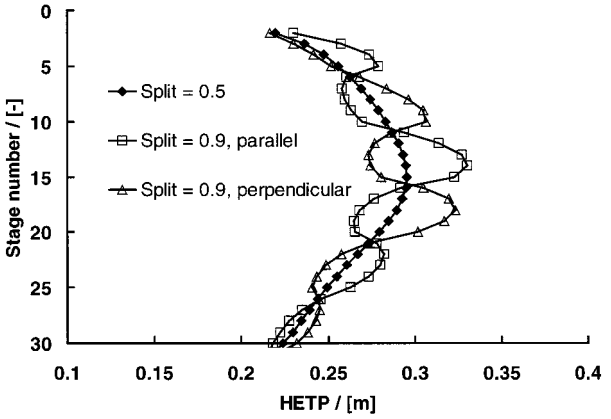

Figure 8. Differential HETPs for structured packing.

To test the above, we have done several calculations for the same binary system outlined above, with a structured packing replacing the dumped packing. We will take a general sheet type packing, with a specific surface area of 300 m^2/m^3, a channel base width of 0.0259 m, and a corrugation angle of 45°. We will use a packed height of 6 m, which is split up into slices of 0.1 m each. The feed specification from the original example was maintained, as was the bottom product flow rate. The reflux ratio was set to 1, to obtain a column diameter in the top section of about 0.8 m. This may be adequately described by a 10 × 10 cell layout pattern, as represented in Figure 5. Mass-transfer coefficients and interfacial areas were calculated with the method of Bravo et al.[18]

Calculations will be done for case Square-2, whereby we will look at three different situations. First, we will assume that splitting in the *x* and *y* directions will be equal. Second, we will look at a case in which we assume that 90% of the flow splits along the packing, assuming the initial maldistribution has the same orientation as the packing, and third, we will look at a similar situation in which the orientation of the initial maldistribution is perpendicular to the orientation of the packing sheets. We further assume that after each set of five stages (0.5 m) the packing orientation changes.

In Figure 8 we see the differential HETPs for the top section of the packing. As can be seen, the packing anisotropy causes the differential HETPs to meander around the differential HETP that is found if the packing would be isotropic. In addition this figure suggests that the initial maldistribution does not disappear completely, as the meandering is still seen in the lower section of the column. When the maldistribution pattern is parallel to the orientation of the sheets in the packing, the HETP is higher than when the orientation is perpendicular. This is in line with our expectations.

The fact that the initial HETP for the perpendicular split is lower than that for the equal split is explained by the fact that, with the 0.9 perpendicular split, the liquid will spread out much more rapidly than when using a 0.5 split.

4.3. Ternary System 1: Methanol−Isopropanol−Water. In the following section we will focus our attention on a nonideal mixture of methanol, 2-propanol

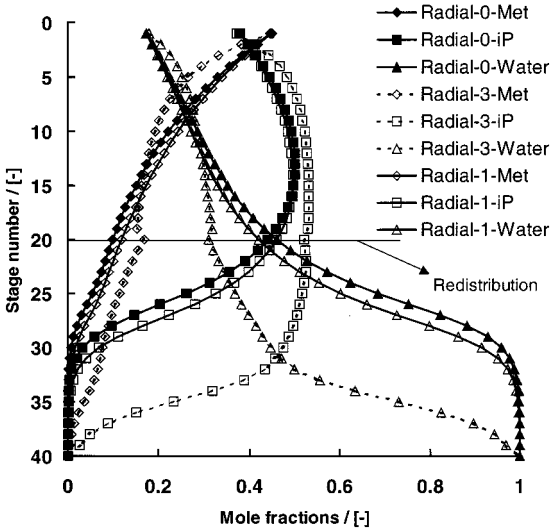

Figure 9. Concentration profiles for a methanol−isopropanol−water column at various maldistribution patterns.

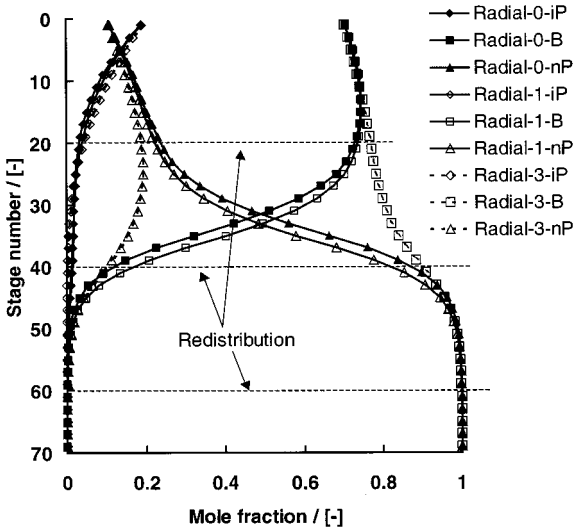

Figure 10. Concentration profiles for a isopropanol−benzene−*n*-propanol column at various maldistribution patterns.

and water. This mixture has one binary azeotrope between 2-propanol, and water. Total reflux calculations were done with this system. The NRTL model was used for the activity coefficients.

Column simulations were done for a packed column with a packing height of 4 m, consisting of 1 in. Raschig rings. The correlations due to Onda et al.[17] were used for calculation of mass transfer coefficients and vapor/liquid interfacial areas. The packed section was split up into 40 slices of 0.1 m each. The flow rates were chosen such that a column diameter of about 1 m was obtained. For investigating the influence of maldistribution of the reflux flow on column behavior, we will use the radial maldistribution patterns as given in Figure 5. The column internal flows were redistributed according to distribution pattern Radial-0 in Figure 5.

Plotted in Figure 9 are the concentration profiles as obtained with cases Radial-0, Radial-1, and Radial-3. As can be seen, the differences are considerable. Although both the values of C_v and *MI* for case Radial-3 are lower than those for case Radial-1, the effects of maldistribution are more pronounced for case Radial-3. Apparently, the indexes do not completely describe what happens in the column. It should be noted here that, in the column under consideration, we are dealing with a system in which, in part of the column (the top section), there is no substantial change in the concentration profiles and, in another section, there is a huge jump over just a relatively small number of "slices". In these cases, minor differences in the top section of the column may work out to have a substantial influence in the bottom part of the column. Obviously, redistribution cannot prevent this behavior, because most of the damage is done in the top section. The influence of redistribution is visible only in the concentration profiles for Radial-3. This is due to the fact that, in the natural flow model, irregularities in the flow profile will be smoothed out along the height of the column and disappear completely if the column is high enough. If the maldistribution is not too severe, the effects will only be felt on a limited number of stages because the natural flow model itself will take care of redistribution.

4.4. Ternary System 2: Isopropanol−Benzene−*n*-Propanol. The isopropanol−benzene−*n*-propanol system also exhibits thermodynamically nonideal behavior. The system has two binary azeotropes, one of which is a low boiling stable node (2-propanol−benzene); the other is a saddle azeotrope between benzene and *n*-propanol. Both azeotropes are connected by a distillation boundary. Total reflux calculations were done for this system, again using the NRTL model.

Column calculations were done for a column with a height of 7 m, packed with 1 in. Raschig rings. The correlations due to Onda et al.[17] were used for calculation of mass-transfer coefficients and interfacial areas. The packed section was split up into 70 slices of 0.1 m each. The flow rates were chosen such that a column diameter of about 1 m was obtained. The radial maldistribution patterns, as shown in Figure 5, were used for the reflux stream. The internal liquid flows were redistributed over the cross-sectional area of the column after 2, 4, and 6 m (at stages 20, 40, and 60).

The observed concentration profiles for cases Radial-0, Radial-1, and Radial-3 are given in Figure 10. Most remarkable here is that, for cases Radial-0 and Radial-1, the bottom of the column consists of pure *n*-propanol, whereas for case Radial-3 the bottom product is pure benzene. Depending on how the reflux is maldistributed, we can apparently obtain different pure products from one single distillation column.

The reason for the observed behavior can be found in the fact that the maldistribution influences the individual component efficiencies. This is illustrated by the relative efficiency differences between *n*-propanol and 2-propanol, given by

$$\Delta(\text{eff}) = \frac{E_{\text{nP}}^{\text{MV}} - E_{\text{iP}}^{\text{MV}}}{E_{\text{nP}}^{\text{MV}}} \tag{37}$$

The Murphree vapor phase efficiencies for each slice are calculated from the results of the nonequilibrium model. The results are presented in Figure 11. Shown here are the relative efficiency differences in the top of the column for cases Radial-0, -1, and -3. As can be seen, there are substantial differences between cases Radial-0 and -1 on one hand and case Radial-3 on the other hand. Pelkonen et al.[19] have already shown that different models can predict different distillation lines. This is due to the fact that mass-transfer interactions may result in changes in the curvature and location of the distillation boundaries. Similar observations are made

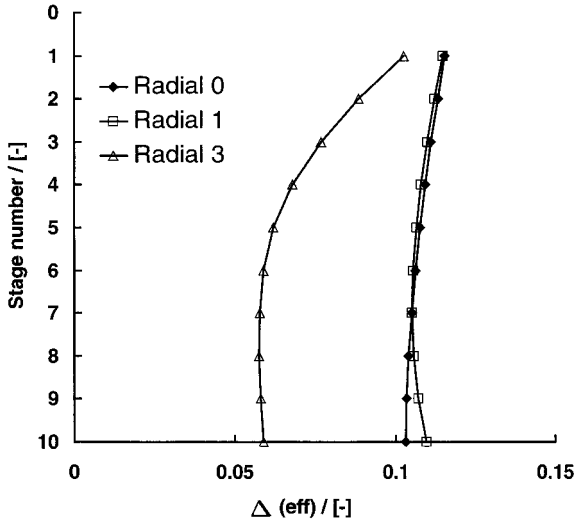

Figure 11. Efficiency differences between isopropanol and benzene in the top section of the column.

by Castillo and Towler,[20] who point out that differences between the efficiencies of different components in a ternary mixture can lead to differences in the curvature of the distillation lines and boundaries.

In their study, Pelkonen et al.[19] limited themselves to modeling packed column behavior without taking maldistribution into account. As illustrated above, differences in maldistribution may also result in changes in the curvature of the distillation boundaries and lines. This means that distillation lines may start in slightly different directions, and possibly on different sides of the distillation boundary, if the initial point is located close to the distillation boundary. This is indeed the case in this example.

To test this conclusion, we have done calculations whereby all the component efficiencies in a contacting cell were set equal to one another. This was done by neglecting the liquid-phase mass-transfer resistance and setting all vapor-phase diffusivities equal. In this case, we will not have the relatively large differences in efficiencies in the top part of the column. As a result, the distillation lines for each individual case will have equal directions at the start, and we find, for all maldistribution cases, that the bottom of the column consists of pure benzene.

The results are summarized in the distillation line map in Figure 12. Here we have plotted the distillation lines for case Radial-0, case Radial-3, and the no-maldistribution case with "equal efficiencies". All distillation lines originate from the same point, which is very close to the distillation boundary. From here the no-maldistribution case goes toward the pure *n*-propanol corner. The other two go toward the pure benzene corner.

In addition, we have tested the influence of redistribution by doing the same calculations as described above assuming no redistribution of liquid. The results were very similar to those presented here. Redistribution does not have a large impact on the outcome of the calculations, because the important part of the column is just a few stages at the top. Differences in maldistribution patterns lead to distillation lines setting off in slightly different directions. Redistribution does not have an impact as it takes place too far from the zone where the differing distillation lines originate.

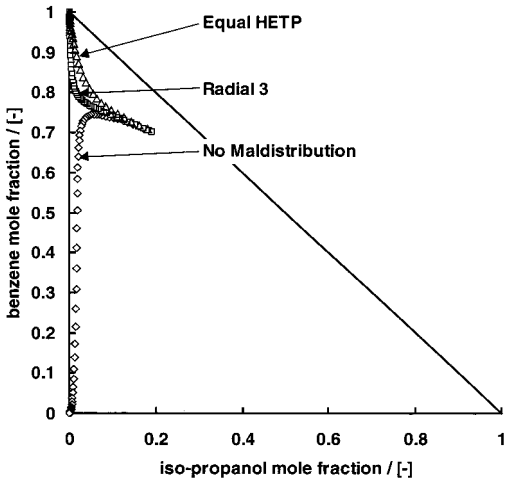

Figure 12. Distillation lines for the isopropanol−benzene−*n*-propanol system.

5. Conclusion

We have developed a nonequilibrium model for studying the effect of flow maldistribution in structured packings. The model consists of a set of mass and energy balances along with a set of mass- and energy-transfer correlations. Maldistribution is treated by means of a zone/stage approach developed and presented by Zuiderweg et al.[1] In this approach, a section of packing is first divided into a number of slices, and each slice is subsequently divided into a number of mixing cells. The size of these cells follows from considerations with respect to radial spreading, as outlined by Hoek et al.,[3] Stikkelman,[4] and Bemer and Zuiderweg.[10]

Calculations for some maldistribution cases have indicated that there is some correspondence between the observed deviations of the efficiencies from "ideal" behavior and the currently available methods for reporting maldistribution, the C_v value and the maldistribution index *MI*. It should, however, be noted that, in some cases, these parameters provide inadequate information. It is generally true that maldistribution results in loss of efficiency, but poorer maldistribution does not necessarily lead to poorer efficiency. Simulations show that, even for binary mixtures, packing HETPs can be a function of the height of the packing.

Efficiencies and HETPs in multicomponent systems tend to be confusing, and the effect of maldistribution on these parameters is ambiguous. We have shown for two ternary systems that different maldistribution patterns can result in substantial differences in column behavior. In some cases, different maldistribution patterns may lead to completely different products from a column. To the best of our knowledge, such an observation, which needs experimental verfication, has not been made before.

Acknowledgment

The authors would like to thank Dr. H. A. Kooijman for assistance in the preparation of this paper. Partial support for our work is provided by BP-Amoco Chemicals and the members of the ChemSep consortium.

Notation

a_k = outside surface area of cell k, m^2
$A_{i,j}$ = thermodynamic interaction parameter, $J \cdot mol^{-1}$

A_t = total cross-sectional area, m^2
C_m = coefficient of variation, unitless
C_v = coefficient of variation, unitless
c = total number of components, unitless
c_t = total concentration, $mol \cdot m^{-3}$
D_r = radial liquid spreading coefficient, m
d_p = nominal packing size, m
E^{MV} = Murphree vapor-phase efficiency, unitless
E^L = energy-transfer rate liquid phase, $J \cdot s^{-1}$
E^V = energy-transfer rate vapor phase, $J \cdot s^{-1}$
F^L = liquid feed rate, $mol \cdot s^{-1}$
F^V = vapor feed rate, $mol \cdot s^{-1}$
f_i^L = liquid feed rate of component i, $mol \cdot s^{-1}$
f_i^V = vapor feed rate of component i, $mol \cdot s^{-1}$
H_k^{CL} = enthalpy of liquid stream leaving cell k, $J \cdot s^{-1}$
H_j^{SL} = enthalpy of liquid stream leaving stage j, $J \cdot s^{-1}$
H_k^{CV} = enthalpy of vapor stream leaving cell k, $J \cdot s^{-1}$
H_j^{SV} = enthalpy of vapor stream leaving stage j, $J \cdot s^{-1}$
HETP = height equivalent of a theoretical plate, m
h^L = liquid side heat-transfer coefficient, $J \cdot K^{-1} \cdot m^{-2} \cdot s^{-1}$
h^V = vapor side heat-transfer coefficient, $J \cdot K^{-1} \cdot m^{-2} \cdot s^{-1}$
H = height of a slice of packing, m
$K_{i,k}$ = vapor−liquid equilibrium constant of component i in cell k, unitless
K^L = liquid splitting factor, unitless
K^V = vapor splitting factor, unitless
K_x = flow splitting factor in x direction, unitless
K_y = flow splitting factor in y direction, unitless
L_k^C = liquid flow rate leaving cell k, $mol \cdot s^{-1}$
L_j^S = liquid flow rate leaving stage j, $mol \cdot s^{-1}$
MI = maldistribution index, unitless
N^L = liquid phase mass-transfer rate, $mol \cdot s^{-1}$
N^V = vapor phase mass-transfer rate, $mol \cdot s^{-1}$
n^Z = number of zones or cells on a stage, unitless
p_j = pressure on stage j, Pa
Q = heat duty, $J \cdot s^{-1}$
R = gas constant, $J \cdot mol^{-1} \cdot K^{-1}$
R = column radius, m
r = radius, m
r_l = cell width, m
r_k^{ai} = inside surface area ratio of cell k, unitless
r_k^{ao} = outside surface area ratio of cell k, unitless
r_a^L = area factor for determination of liquid flows to cells, unitless
r_a^V = area factor for determination of vapor flows to cells, unitless
r_f^L = factor for determination of liquid feed to a cell, unitless
r_f^V = factor for determination of vapor feed to a cell, unitless
r_j^L = ratio of liquid side stream to stage liquid flow rate, unitless
r_j^V = ratio of vapor side stream to stage vapor flow rate, unitless
T = temperature, K
u = velocity, $m \cdot s^{-1}$
$\bar{u}$ = average velocity, averaged over whole cross-sectional area, $m \cdot s^{-1}$
$\bar{u}_i$ = average velocity, averaged over cell i and neighboring cells, $m \cdot s^{-1}$
V_k^C = vapor flow rate leaving cell k, $mol \cdot s^{-1}$
V_j^S = vapor flow rate leaving stage j, $mol \cdot s^{-1}$
x = volume fraction of liquid, unitless
$x_{i,k}^C$ = liquid mole fraction of component i in cell k, unitless
$x_{i,j}^S$ = liquid mole fraction of component i on stage j, unitless
$y_{i,k}^C$ = vapor mole fraction of component i in cell k, unitless
$y_{i,j}^S$ = vapor mole fraction of component i on stage j, unitless
z = bed depth or bed height, m
z_l = cell height, m

Greek Symbols

Δ(eff) = relative efficiency difference, defined by eq 37, unitless
$\delta_{i,j}$ = 1 if i and j are neighbors; otherwise 0, unitless
η = dimensionless film coordinate, unitless
$\kappa_{i,l}$ = binary pair mass-transfer coefficient components i and j, $m \cdot s^{-1}$
μ_i = chemical potential of component i, $J \cdot mol^{-1}$
ρ^L = liquid-phase density, $kg \cdot m^{-3}$
ρ^V = vapor-phase density, $kg \cdot m^{-3}$
σ = surface tension, $N \cdot m^{-1}$

Superscripts

* = indicating equilibrium
C = cell property or quantity
I = interface property or quantity
L = liquid property or quantity
MV = Murphree vapor phase
S = stage property or quantity
V = vapor property or quantity
Z = zone property or quantity

Subscripts

i = component index
iP = 2-propanol
j = stage index
k = cell or zone index
nP = *n*-propanol

Literature Cited

(1) Zuiderweg, F. J.; Kunesh, J. G.; King, D. W. A model for the calculation of the effect of maldistribution on the efficiency of a packed column. *Trans. IChemE* **1993**, *71*, *part A*, 38.

(2) Porter, K. E.; Jones, M. C. Theoretical prediction of liquid distribution in a packed column with wall effect. *Trans. IChemE* **1963**, *41*, 240.

(3) Hoek, P. J.; Wesselingh, J. A.; Zuiderweg, F. J. Small scale and large scale liquid maldistribution in packed columns. *Chem. Eng. Res. Des.* **1986**, *64*, 431.

(4) Stoter, C. F. Modelling of maldistribution in structured packigns: From detail to column design. Ph.D. Dissertation, Delft Technical University, Delft, The Netherlands, 1993.

(5) Stikkelman, R. M. Gas and liquid maldistributions in packed columns. Ph.D. Dissertation, Delft Technical University, Delft, The Netherlands, 1989.

(6) Stoter, C. F.; Olujic, Z.; Graauw, J. de. Modelling of hydraulic and separation performance of large diameter columns containing structured packings. *IChemE Symp. Ser.* **1992**, *128*, A201.

(7) Billingham, J. F.; Bonaquist, D. P.; Lockett, M. J. Characterization of the performance of packed distillation column liquid distributors. *IChemE Symp. Ser.* **1997**, *142*, 841.

(8) Perry, D.; Nutter, D. E.; Hale, A. Liquid distribution for optimum packing performance. *Chem. Eng. Prog.* **1990**, *86*, 30.

(9) Edwards, D. P.; Krishnamurthy, K. R.; Potthoff, R. W. Development of an improved method to quantify maldistribution and its effect on structured packing column performance. AIChE annual meeting, Miami Beach, FL, 1998.

(10) Bemer, G. G.; Zuiderweg, F. J. Radial liquid spread and maldistribution in packed columns under different wetting conditions. *Chem. Eng. Sci.* **1978**, *33*, 1637.

(11) Nawrocki, P. A.; Xu, Z. P.; Chuang, K. T. Mass transfer in structured corrugated packing. *Can. J. Chem. Eng.* **1991**, *69*, 1336.

(12) Wesselingh, J. A. Nonequilibrium modeling of distillation. *IChemE Symp. Ser.* **1997**, *142*, 1.

(13) Krishna, R.; Wesselingh, J. A. The Maxwell-Stefan Approach to Mass Transfer. *Chem. Eng. Sci.* **1997**, *52*, 861.

(14) Taylor, R.; Krishna, R. *Multicomponent Mass Transfer*; Wiley: New York, 1993.

(15) Higler, A. P.; Krishna, R.; Taylor, R. A nonequilibrium cell model for multicomponent reactive separation processes. Submitted for publication in *AIChE J*.

(16) Taylor, R.; Kooijman, H. A.; Hung, J. S. A second generation nonequilibrium model for computer simulation of multicomponent separation processes. *Comput. Chem. Eng.* **1994**, *18*, 205.

(17) Onda, K.; Takeuchi, H.; Okumoto, Y. Mass transfer coefficients between gas and liquid phases in packed columns. *J. Chem. Eng. Jpn.* **1968**, *1*, 56.

(18) Bravo, J. L.; Rocha, J. A.; Fair, J. R. Distillation columns containing structured packings: A comprehensive model for their performance. 1. Hydraulic models. *Ind. Eng. Chem. Res.* **1992**, *32*, 641.

(19) Pelkonen, S.; Kaesemann, R.; Gorak, A. Distillation lines for multicomponent separation in packed columns: Theory and comparison with experiments. *Ind. Eng. Chem. Res.* **1997**, *36*, 5392.

(20) Castillo, F. J. L.; Towler, G. P. Influence of multicomponent mass transfer on homogeneous azeotropic distillation. *Chem. Eng. Sci.* **1998**, *53*, 963.

Received for review April 12, 1999
Revised manuscript received June 29, 1999
Accepted July 9, 1999

IE990261L